Influence of nonlinear thermocapillary effect on Marangoni patterns in thin film

Alexander B. Mikishev [*]
Department of Engineering Technology, Sam Houston State University, Huntsville, Texas 77341, USA

Alexander A. Nepomnyashchy [†]
Department of Mathematics, Technion-Israel Institute of Technology, Haifa 32000, Israel

(Received 17 January 2020; accepted 22 April 2020; published 8 May 2020)

We consider the long-wave Marangoni convection in a horizontally oriented heated thin liquid layer with weak heat flux from the free surface. Two modes of instability are possible in this problem: monotonic and oscillatory. The system of nonlinear evolution equations is modified for the case when the surface tension is a nonlinear function of temperature determined by a set of coefficients in the Taylor series expansion about the surface temperature. The coefficients which are used are taken mainly from experimental data. In the case of monotonic instability, we investigate the influence of nonlinear temperature dependence of the surface tension on the stability of roll, square, and hexagonal patterns. In the case of oscillatory instability, we consider the stability of single traveling waves and traveling rectangles.

DOI: 10.1103/PhysRevFluids.5.054001

I. INTRODUCTION

Thermocapillary convection is an important mechanism of heat and mass transfer in many physical processes with open interfaces. This kind of convection is a liquid's motion generated by temperature inhomogeneity at a liquid-liquid or liquid-gas interfaces which induces the gradient of surface tension. In the reduced gravity environment the role of the thermocapillary effect increases compared to buoyancy. The theoretical description of this phenomenon is far from being complete.

The surface tension of liquids typically decreases with temperature, [1]. However, the experiments with dilute aqueous solutions of n-heptanol and n-hexanol performed on the Earth [2] and under microgravity conditions [3–5] show a nonlinear behavior of the surface tension with the change of temperature. In these experiments, the surface tension had a minimum at some temperature. At the same time, measurements for binary metallic alloys [6,7] show that the surface tension can have also a maximum at some temperatures. These experiments awoke a lot of numerical and analytical works on the subject, see Refs. [8–11].

We are interested especially in those of them that describe the behavior of thin liquid films. Cloot and Lebon, [8], considered the Bénard-Marangoni problem using the linear stability theory, the weakly nonlinear analysis and the energy method. The stability analysis of different convective patterns with square, rectangular, and hexagonal planforms showed that only hexagons are stable with respect to small disturbances. The nonlinear spatiotemporal evolution of a thin liquid layer with quadratic dependence of the surface tension on the temperature was examined by Oron and Rosenau [10]. For the disturbances of the liquid thickness, they obtained the evolution equation

[*]Corresponding author: amik@shsu.edu
[†]nepom@technion.ac.il

of the Cahn-Hillard type. While in the case of a linear dependence of the surface tension on the temperature the film always ruptures, Oron and Rosenau found stable steady states with perfectly continuous interfaces evolving out of arbitrary small perturbations of the interface.

The majority of the papers on Marangoni convection in a layer with a poorly conducting upper boundary was carried out with the wave number $k = O(\mathrm{Bi}^{1/4})$. However, Podolny *et al.* [12] for the first time, as far as we know, treated the asymptotics $k = O(\mathrm{Bi}^{1/2})$ considering the onset of Marangoni convection in binary liquids and found under this assumption the oscillatory mode of instability as well as monotonic one. Later Shklyaev with coauthors [13], investigated in details these modes of instability in the case of a weak heat flux from the free liquid surface of the three-dimensional (3D) thin layer. For the oscillatory mode, supercritical bifurcation of different wave patterns is possible.

The effect of temperature variation of surface tension on the linear Marangoni instability in the case of $k \sim \mathrm{Bi}^{1/2}$ was discussed in Ref. [14]. Here we consider the influence of the nonlinearity of the surface tension's temperature dependence on the nonlinear development of the Marangoni convection and pattern selection for monotonic and oscillatory instabilities in a thin liquid film.

II. PROBLEM FORMULATION

We consider a horizontally infinite 3D thin liquid layer (with a mean thickness d_0) of an incompressible liquid with the thermal diffusivity χ, the kinematic viscosity ν, the density ρ, and the dynamic viscosity $\eta = \rho\nu$. The liquid is confined between a rigid lower plane, located at $z = 0$, and a free deformable upper surface. It is assumed that the z axis is directed vertically upward. The layer is heated from below in the gravity field and it is subjected to a transverse temperature gradient $-a$ ($a > 0$).

Let us rescale the variables of the problem using the following characteristic units: the length unit is d_0, the time unit is d_0^2/χ, the velocity unit is χ/d_0, the temperature unit is ad_0, and the pressure unit is $\rho\nu\chi/d_0^2$. We obtain the following boundary value problem:

$$\nabla \cdot \mathbf{v} = 0, \tag{1}$$

$$P^{-1}[\mathbf{v}_t + (\mathbf{v}\cdot\nabla)\mathbf{v}] = -\nabla p + \nabla^2\mathbf{v} - G\mathbf{e}_z, \tag{2}$$

$$T_t + \mathbf{v}\cdot\nabla T = \nabla^2 T, \tag{3}$$

$$\mathbf{v} = 0, \quad T_z = -1, \quad \text{at} \quad z = 0, \tag{4}$$

$$h_t = w - \mathbf{u}\cdot\nabla h, \tag{5}$$

$$\begin{aligned} -p + \frac{2}{1+h_x^2+h_y^2}\left[u_x\left(h_x^2-1\right) + v_y\left(h_y^2-1\right) - h_x(u_z+w_x) + (u_y+v_x)h_xh_y - (w_y+v_z)h_y\right] \\ = \Sigma\left[h_{xx}\left(1+h_y^2\right) + h_{yy}\left(1+h_x^2\right) - 2h_xh_yh_{xy}\right]\left(1+h_x^2+h_y^2\right)^{-3/2}, \end{aligned} \tag{6}$$

$$\begin{aligned} 2(w_z-u_x)h_x - (u_y+v_x)h_y - h_xh_y(v_z+w_y) + (u_z+w_x)\left(1-h_x^2\right) \\ = -M(T_x + h_xT_z)\sqrt{1+h_x^2+h_y^2}, \end{aligned} \tag{7}$$

$$\begin{aligned} 2(w_z-v_y)h_y - (u_y+v_x)h_x - h_xh_y(u_z+w_x) + (v_z+w_y)\left(1-h_y^2\right) \\ = -M(T_y + h_yT_z)\sqrt{1+h_x^2+h_y^2}, \end{aligned} \tag{8}$$

$$\mathbf{n}\cdot\nabla T = -\mathrm{Bi}T, \quad \text{at} \quad z = h(x,y,t). \tag{9}$$

Here $\mathbf{v} = (\mathbf{u}, w)$ is the velocity field ($\mathbf{u} = (u, v)$ is the horizontal velocity vector field, w is a vertical velocity component), p is the difference between the liquid pressure and the atmospheric one, T is the difference between the temperature of the liquid and that of the gas above the liquid film, h is the local thickness of the layer, $\mathbf{e}_z$ is the unit vector directed upward, $\mathbf{n} = (-h_x, -h_y, 1)(1 + h_x^2 + h_y^2)^{-1/2}$ is the unit vector normal to the surface, $\nabla = (\partial_x, \partial_y, \partial_z)$, a subscript denotes the corresponding derivative. The problem contains the following nondimensional parameters:

$$P = \nu/\chi, \quad G = g d_0^3/\nu\chi, \quad \Sigma = \sigma d_0/\chi\eta, \quad \mathrm{Bi} = q d_0/\lambda,$$

which are the Prandtl number, the modified Galileo number (usual form of the Galileo number is $G = g d_0^3/\nu^2$), the inverse capillary number, and the Biot number, respectively; here q is the heat transfer coefficient and λ is the heat conductivity of the liquid. Also we introduce the Marangoni number,

$$M(x, y, t) = -\sigma_T [T_0(x, y, t)] a d_0^2/\eta\chi,$$

where $T_0(x, y, t) = T(x, y, z, t)|_{z=h(x,y,t)}$ is the surface temperature. Let us emphasize that because of the nonlinear dependence of the surface tension on temperature, M is generally not constant but a variable determined by the distribution of the surface temperature. Here the surface tension $\sigma = \sigma(T)$ is a function of temperature specified later, $\sigma_T = d\sigma(T)/dT$.

The problem has a well-known basic solution (see Ref. [12])

$$h_b = 1, \quad T_b = -z + \frac{1 + \mathrm{Bi}}{\mathrm{Bi}}, \quad p_b = -G(z - 1). \tag{10}$$

In the present paper we consider the nonlinear evolution of long-wave perturbations and pattern selection for the monotonic and oscillatory instability modes.

III. LONG-WAVE APPROXIMATION

To analyze the evolution of large-scale instabilities in the problem we rescale the variables introducing the coordinates

$$X = \epsilon x, \quad Y = \epsilon y, \quad Z = z, \tag{11}$$

the time

$$\tau = \epsilon^2 t, \tag{12}$$

and the velocity components

$$\mathbf{U} = \epsilon^{-1}\mathbf{u}, \quad W = \epsilon^{-2} w. \tag{13}$$

Here parameter $\epsilon \ll 1$ can be defined as a ratio between the mean layer thickness d_0 and typical horizontal scale of the problem. Following Ref. [13], we impose

$$\Sigma = \epsilon^{-2} S. \quad \mathrm{Bi} = \epsilon^2 \beta. \tag{14}$$

The latter assumption means that the disturbances with small wave numbers $k = O(\mathrm{Bi}^{1/2})$ are considered. Other dimensionless parameters, such as the Prandtl number, the Galileo number, and the Marangoni number, are scaled as $O(1)$. We assume that the disturbances of temperature, T, and the thickness of the layer, h, are $O(1)$. To derive the evolution equations we expand the dependent variables of the problem as

$$(h, \mathbf{U}, W, p) = (H_0, \mathbf{U_0}, W_0, \Pi_0) + \epsilon^2 (H_2, \mathbf{U_2}, W_2, \Pi_2) + \ldots, \tag{15}$$

$$T = -z + \mathrm{Bi}^{-1} + F_0 + \epsilon^2 F_2 + \ldots. \tag{16}$$

Substituting the expansions into the system of equations and boundary conditions and collecting the terms of the same order of ϵ we obtain a sequence of evolution problems. Solving the problem obtained at the leading order of ϵ, we find the following solution:

$$\Pi = P(X, Y, \tau) - GZ, \quad F = F(X, Y, \tau), \tag{17}$$

$$\mathbf{U} = \frac{Z}{2}(Z - 2H)\nabla P - M\nabla(F - H)Z, \tag{18}$$

$$W = -\frac{Z^3}{6}\nabla^2 P + \frac{Z^2}{2}\{\nabla \cdot (H\nabla P) + M\nabla^2(F - H)\}. \tag{19}$$

Here the subscript 0 is omitted, $P = GH - S\nabla^2 H$, $F - H$ has a meaning of the temperature perturbation at the free surface, $\nabla = (\partial_X, \partial_Y, 0)$. The kinematic condition $H_\tau = -\nabla \cdot \int_0^H \mathbf{U} dZ$ gives the evolution equation for the layer thickness:

$$H_\tau = \nabla \cdot \left[\frac{H^3}{3}\nabla P + \frac{H^2}{2}M\nabla(F - H)\right] = \nabla \cdot \mathbf{Q}. \tag{20}$$

Here the vector $-\mathbf{Q}$ has a meaning of the longitudinal flux of a liquid integrated across the layer. The first term on the right-hand side of the equation describes the damping of the surface deflection due to gravity and surface tension, the second term describes the influence of thermocapillary flow.

The evolution equation for the temperature is obtained from the solvability condition of the problem at the second order of ϵ:

$$HF_\tau = \nabla \cdot \left[\frac{H^4}{8}\nabla P + \frac{H^3}{6}M\nabla(F - H) + H\nabla F\right] + \mathbf{Q} \cdot \nabla(F - H) - \frac{1}{2}(\nabla H)^2 - \beta(F - H). \tag{21}$$

Here the first two terms in the right-hand side and the fourth one describe the advective heat transfer by the flow, the third term describes heat conductivity in the longitudinal direction, the fifth and sixth terms are responsible for heat losses from the free surface. Recall that the Marangoni number M is the function of the surface temperature deviation $\Theta = F - H$. We take this dependence $M(\Theta)$ on the basis of experimental data. This dependence influences the nonlinear behavior of disturbances. A similar approach was used by authors to derive the system of evolution equations for long-wave Marangoni convection in the presence of insoluble surfactant, see Refs. [15,16].

Equations (20) and (21) have the obvious base solution, $H^{(b)} = 1$, $F^{(b)} = 1$, hence $\Theta^{(b)} = 0$, and the corresponding Marangoni number for this solution is $M^{(b)} = M|_{\Theta=0}$.

IV. MARANGONI NUMBER AS NONLINEAR FUNCTION OF TEMPERATURE

We consider the nonlinear dynamics of large-scale perturbations near one of the critical Marangoni numbers. These numbers are found by the linear analysis of the problem performed in Ref. [13], that predicts

$$M_m^{(b)}(K) = \frac{48(\beta + K^2)(G + SK^2)}{K^2(72 + G + SK^2)} \tag{22}$$

as the marginal Marangoni number for monotonic instability mode and

$$M_o^{(b)}(K) = 3 + 3\beta/K^2 + G + SK^2 \tag{23}$$

as the marginal Marangoni number for oscillatory instability mode. Note that here $K = k/\epsilon = O(1)$ is the *rescaled* wave number, while the original wave number $k = O(\epsilon) = O(\mathrm{Bi}^{1/2})$. The critical values of these numbers are taken at the minima of the instability curves $M^{(b)} = M^{(b)}(K)$,

$$K_c^m = \left\{ \frac{\beta SG + [72\beta SG(72 + G - \beta S)]^{1/2}}{S(72 - \beta S)} \right\}^{1/2}, \tag{24}$$

$$K_c^o = (3\beta)^{1/4}. \tag{25}$$

Let us consider the nonlinear evolution of disturbances near the instability threshold, i.e., assume that the actual Marangoni number for the base state $M^{(b)} = M(0) = m_0^*$ is close to the critical monotonic or oscillatory Marangoni number m_0 [$m_0 = M_m^{(b)}$ or $m_0 = M_o^{(b)}$], $|m_0^* - m_0| \ll 1$. Suppose that the disturbances evolving on the background of the base state are small, and they grow or decay slowly.

For description of the evolution of small disturbances on the background of the base state, we introduce expansions in powers of a small parameter δ:

$$H = 1 + \delta h_1 + \delta^2 h_2 + \delta^3 h_3 + \ldots, \tag{26}$$

$$F = 1 + \delta f_1 + \delta^2 f_2 + \delta^3 f_3 + \ldots. \tag{27}$$

The relation between δ and $m_0^* - m_0$ depends on the type of bifurcation and it will be discussed later. As mentioned before, the Marangoni number depends on the surface tension that is a function on temperature. We expand the Marangoni number into Taylor series around the undisturbed value of temperature of the free surface of the liquid, i.e.,

$$M(\Theta) = m_0^* + m_1\Theta + m_2\Theta^2 + \ldots, \tag{28}$$

where m_0^* is the Marangoni number in the motionless state, $m_1 = dM/d\Theta$, $m_2 = (1/2)d^2M/d\Theta^2$, etc.

Taking into account (26) and (27), we obtain:

$$M = m_0^* + \delta m_1(f_1 - h_1) + \delta^2[m_1(f_2 - h_2) + m_2(f_1 - h_1)^2] + \ldots. \tag{29}$$

Substituting (26), (27), and (29) into the system (20) and (21), and collecting terms of the same order of δ, we obtain at the leading order the linear problem for h_1 and f_1, discussed in Ref. [13]:

$$h_{1,\tau} = \nabla^2\left[\frac{1}{3}P_1 + \frac{m_0}{2}(f_1 - h_1)\right], \tag{30}$$

$$f_{1,\tau} = \nabla^2\left[\frac{1}{8}P_1 + \frac{m_0}{6}(f_1 - h_1) + f_1\right] - \beta(f_1 - h_1), \tag{31}$$

where $P_1 = Gh_1 - S\nabla^2 h_1$. For the solutions in the form $\exp(r\tau + iKX)$ we reproduce the results of the linear stability theory. Taking $r = 0$, we obtain the monotonic instability boundary. For this instability we have $m_0^{(\mathrm{mon})} = M_m^{(b)}$ [see (22)] and the minimum at a finite value of K exists only if $\beta S < 72$; otherwise, the minimum of the leading order of Marangoni number, m_0, is the well-known Pearson's minimum $M_{m,c}^{(b)} = 48$ approached when $K \to \infty$. The reason for the divergence of the *rescaled* wave number K is that the minimum of the neutral curve is now located in the region $k \sim B^{1/4} \gg B^{1/2}$, in accordance with the Pearson's theory.

For the oscillatory mode of instabilities the marginal stability curve is determined by the condition $\mathrm{Re}(r) = 0$; one obtains $m_0^{(\mathrm{osc})} = M_o^{(b)}$ [see (23)]. The imaginary part of the growth rate for the threshold of the oscillatory instability equals

$$\omega = \mathrm{Im}(r) = \frac{K^2}{12}\sqrt{(72 + G + SK^2)\left[m_0^{(\mathrm{mon})} - m_0^{(\mathrm{osc})}\right]}. \tag{32}$$

In calculation presented below the appropriate values of m_0 are positive, however, values of m_1 and m_2 can be both positive and negative. We take the parameters m_1 and m_2 mainly from the experimental data [3,4,17]. These data were obtained investigating the properties of diluted aqueous solutions of h-heptanol (6×10^{-2} molal) and of n-hexanol (4×10^{-2} molal), or long chain alcohol solutions with six and nine carbon atoms. The experimental data from the papers were digitilized and fitted by the empirical law as a surface tension function on temperature. For the simulation we choose the following sets of parameters: (i) the linear dependence of the surface tension function on temperature, $m_0 = M(K_c)$, $m_1 = m_2 = 0$; (ii) $m_1 = dM/dT = -\sigma_{TT} a d_0^2/(\eta\chi) = m_0(d^2\sigma/dT^2)/(d\sigma/dT) = 0.2m_0$, $m_2 = (1/2)d^2M/dT^2 = -\sigma_{TTT} a d_0^2/(\eta\chi) = m_0(1/2)(d^3\sigma/dT^3)/(d\sigma/dT) = 0$; (iii) $m_1 = 0.13m_0$, $m_2 = -0.08m_0$; and (iv) $m_1 = -0.1m_0$, $m_2 = 0.05m_0$.

V. WEAKLY NONLINEAR ANALYSIS OF MONOTONIC MODE

Here we consider the neighborhood of $M_m^{(b)}$. For the computations the wave number will be taken equal to the critical one, $K = K_c^m$ [see (24)]. We consider spatially-periodic patterns corresponding to two lattices in the Fourier space: square lattice and hexagonal lattice.

A. Squares and rolls

As the results of Ref. [13] show, square and roll patterns appear by a pitchfork bifurcation, hence we take in Eq. (29) $m_0^* = m_0 + \delta^2 m_{02}$, $m_0 = m_0^{(\mathrm{mon})}$, and introduce the "slow" timescale, $\tau_2 = \delta^2\tau$, so that

$$\partial_\tau = \delta^2 \partial_{\tau_2}.$$

Here parameter δ is the same expansion parameter as in (26) and (27). The solution of (30) and (31) is presented in the forms of squares or rolls as

$$h_1 = A_1(\tau_2)\cos(KX) + B_1(\tau_2)\cos(KY), \tag{33}$$

$$f_1 = \alpha A_1(\tau_2)\cos(KX) + \alpha B_1(\tau_2)\cos(KY), \tag{34}$$

where $\alpha = 1 - 2(G + SK^2)/3m_0$. Here $A_1(\tau_2)$ and $B_1(\tau_2)$ are real amplitude functions, which describe the planform. They depend only on the "slow time" τ_2, but not on the "fast time" $\tau_0 = \tau$. The planform is rolls when either $B_1 = 0$, $A_1 \neq 0$ or $A_1 = 0$, $B_1 \neq 0$. We have squares, when $A_1 = B_1$.

At the second order in δ we obtain

$$\nabla^2\left[\frac{1}{3}P_2 + \frac{m_0}{2}(f_2 - h_2)\right] = -\nabla\left[h_1\nabla P_1 + m_0 h_1 \nabla(f_1 - h_1) + \frac{m_1}{2}(f_1 - h_1)\nabla(f_1 - h_1)\right], \tag{35}$$

$$\begin{aligned}\nabla^2\left[\frac{1}{8}P_2 + \frac{m_0}{6}(f_2 - h_2) + f_2\right] - \beta(f_2 - h_2) \\ = -\nabla(h_1\nabla f_1) + \frac{1}{2}(\nabla h_1)^2 - \frac{1}{2}\nabla(h_1\nabla P_1) - \frac{1}{3}\nabla(f_1 - h_1)\nabla P_1 \\ - \frac{m_0}{2}[\nabla f_1 \nabla(f_1 - h_1) + h_1\nabla^2(f_1 - h_1)] - \frac{m_1}{6}\nabla[(f_1 - h_1)\nabla(f_1 - h_1)].\end{aligned} \tag{36}$$

Here $P_2 = Gh_2 - S\nabla^2 h_2$. The solution of system (35) and (36) can be found in the form

$$h_2 = A_2(\tau_2)\cos(2KX) + B_2(\tau_2)\cos(2KY) + D_2(\tau_2)\cos(KX)\cos(KY), \tag{37}$$

$$f_2 = F_{02}(\tau_2) + C_1(\tau_2)\cos(2KX) + C_2(\tau_2)\cos(2KY) + C_3(\tau_2)\cos(KX)\cos(KY). \tag{38}$$

The coefficients A_2, B_2, D_2, F_{02}, C_1, C_2, and C_3 are given in the Appendix.

At the third order the system looks as

$$\nabla^2\left[\frac{1}{3}P_3+\frac{m_0}{2}(f_3-h_3)\right]=\partial_{\tau_2}h_1-\nabla\cdot\left[h_1\nabla P_2+\left(h_1^2+h_2\right)\nabla P_1\right]-\frac{m_{02}}{2}\nabla^2(f_1-h_1)$$
$$-\frac{m_0}{2}\nabla\cdot\left[h_1^2\nabla(f_1-h_1)\right]-m_0\nabla\cdot[h_1\nabla(f_2-h_2)+h_2\nabla(f_1-h_1)]$$
$$-m_1\nabla\cdot[h_1(f_1-h_1)\nabla(f_1-h_1)]$$
$$-\frac{m_1}{2}\nabla^2[(f_1-h_1)(f_2-h_2)]-\frac{m_2}{2}\nabla\cdot[(f_1-h_1)^2\nabla(f_1-h_1)], \quad (39)$$

$$\nabla^2\left[\frac{1}{8}P_3+\frac{m_0}{6}(f_3-h_3)+f_3\right]-\beta(f_3-h_3)$$
$$=\partial_{\tau_2}f_1+\nabla h_1\cdot\nabla h_2-\nabla\cdot(h_1\nabla f_2+h_2\nabla f_1)-\frac{1}{3}\nabla P_2\cdot\nabla f_1-\frac{3}{4}\nabla\cdot\left(h_1^2P_1\right)$$
$$-\nabla P_1\cdot\left(h_1\nabla f_1+\frac{1}{3}\nabla f_2\right)-\frac{1}{2}\nabla\cdot(h_1\nabla P_2+h_2\nabla P_1)-\frac{m_{02}}{6}\nabla^2(f_1-h_1)$$
$$-m_0\left\{h_1[\nabla(f_1-h_1)]^2+\frac{1}{2}\nabla\cdot\left[\left(h_1^2+h_2\right)\nabla(f_1-h_1)\right]+\frac{1}{2}h_1\nabla^2(f_2-h_2)\right.$$
$$\left.+\nabla f_1\cdot\nabla(f_2-h_2)-\frac{1}{2}\nabla h_1\cdot\nabla(f_2-h_2)\right\}$$
$$-\frac{m_1}{2}\left\{\nabla\cdot[h_1(f_1-h_1)\nabla(f_1-h_1)]+(f_1-h_1)[\nabla(f_1-h_1)]^2\right.$$
$$\left.+\frac{1}{3}\nabla^2[(f_1-h_1)(f_2-h_2)]\right\}-\frac{m_2}{6}\nabla\cdot[(f_1-h_1)^2\nabla(f_1-h_1)]. \quad (40)$$

The elimination of the secular terms in the system of the third order using the solvability condition leads to a set of two Landau equations in the form:

$$\frac{dA_1}{d\tau_2}=\kappa_0A_1+\kappa_1A_1^3+\kappa_2A_1B_1^2, \quad (41)$$
$$\frac{dB_1}{d\tau_2}=\kappa_0B_1+\kappa_1B_1^3+\kappa_2A_1^2B_1. \quad (42)$$

The coefficient $\kappa_0=(dr/dM)m_{02}$ is positive in the supercritical region ($m_{02}>0$) and negative in the subcritical region ($m_{02}<0$), where r is the growth rate of the linear problem, see Ref. [13],

$$\kappa_0=\frac{K^4(72+G+SK^2)^2m_{02}}{48[(2G+27)SK^4+S^2K^6+9(24-5G)\beta]+K^2[216+G(G+27)-45S\beta)]}. \quad (43)$$

Coefficients κ_1 and κ_2 depend on m_0, m_1, and m_2 and their values determine the pattern stability. There are three relevant combinations of κ_1 and κ_2 that determine the type of bifurcation, see Ref. [18].

The steady solutions of (41) and (42) are the motionless state ($A=B=0$), the roll planform (one of A_1 or B_1 is zero) and the square planform ($A_1^2=B_1^2\neq 0$). The planform selection is determined by the signs of κ_1, $\kappa_1-\kappa_2$, and $\kappa_1+\kappa_2$. If $\kappa_1>0$, then the rolls' solution bifurcates into subcritical region, and it is unstable. If $\kappa_1+\kappa_2>0$, then the solution corresponding to squares bifurcates into subcritical region, and it is unstable. In both cases the weakly nonlinear approach fails to find stable solutions of system (20) and (21). If both $\kappa_1>0$ and $\kappa_1+\kappa_2$ are negative, then the solutions corresponding to the roll and square patterns exist in the supercritical region ($m_{02}>0$). If $\kappa_1-\kappa_2>0$, then the roll pattern is stable; if $\kappa_1-\kappa_2<0$, then the square pattern is stable. In

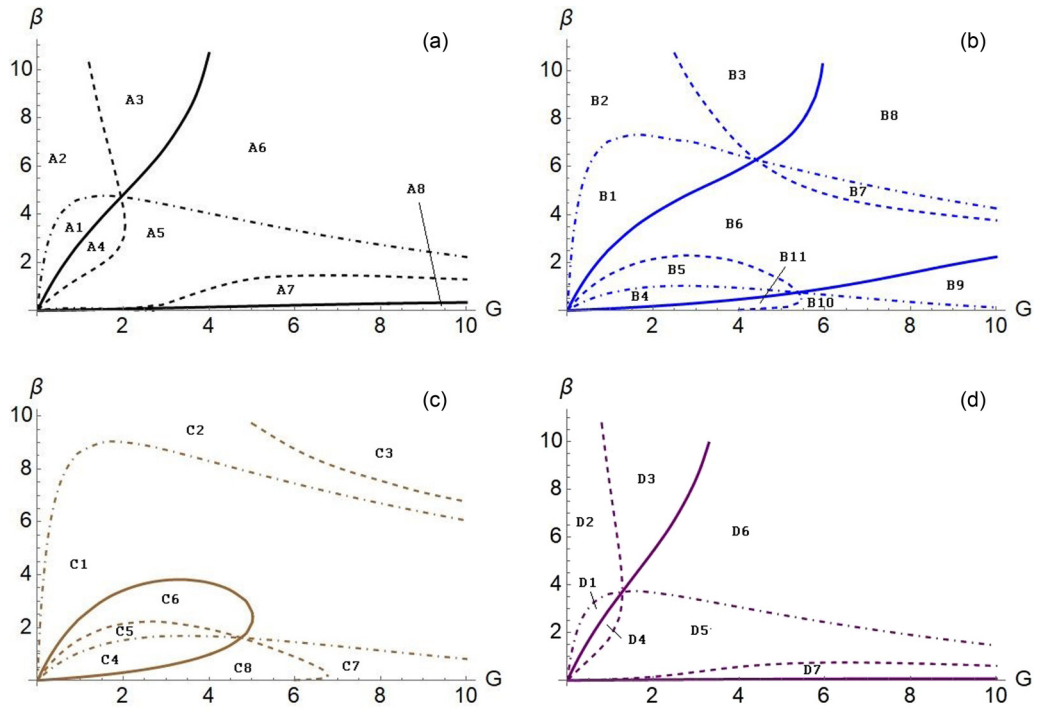

FIG. 1. Pattern selection domains for square lattice of monotonic mode for (a) $m_1 = m_2 = 0$ (linear case). (b) $m_1 = 0.2m_0$ and $m_2 = 0$, (c) $m_1 = 0.3m_0$ and $m_2 = -0.15m_0$, and (d) $m_1 = -0.1m_0$ and $m_2 = 0.05m_0$. Here the solid line is for $\kappa_1 = 0$, the dashed line is for $\kappa_1 + \kappa_2 = 0$, and the dot-dashed line is for $\kappa_1 - \kappa_2 = 0$.

all the computations presented below, without loss of generity, we take $S = 1$. That corresponds to definition of $\epsilon = \Sigma^{-1/2}$.

Figure 1 represents the diagrams of stability domains on the square lattice for monotonic mode at fixed values of m_1 and m_2. Figure 1(a) is the case of linear surface tension ($m_0 = M_m^{(b)}(K_c^m)$ and $m_1 = m_2 = 0$). This case was investigated by Shklyaev *et al.* [13]. Figure 1(b) is for case (i), Fig. 1(c) is for case (ii), and Fig. 1(d) is for case (iii), respectively. Here the solid lines are boundaries between supercritical and subcritical bifurcations for rolls, $\kappa_1 = 0$. The dashed lines are similar boundaries for squares, $\kappa_1 + \kappa_2 = 0$, and the dotted lines correspond to $\kappa_1 = \kappa_2$ and separate the regions of stable rolls and stable squares. Each diagram map is divided by regions: Figure 1(a) has regions from A1 to A8, Fig. 1(b) has regions from B1 to B11, Fig. 1(c) has regions from C1 to C8, and Fig. 1(d) has regions from D1 to D7. All results are combined in the Table I. Those results demonstrate the change of the selected planforms depending on the nonlinearity of the surface tension function. The comparison of Fig. 1(d) with Fig. 1(a) shows that for a certain combination of coefficients m_1 and m_2 one can neglect the effect of nonlinear surface tension function.

B. Hexagons

The dynamical system (20) and (21) includes quadratic nonlinearities and, therefore, preferred planform of the stationary patterns is *a hexagonal* pattern, see Ref. [19]. Because the bifurcation of the hexagonal solution is transcritical, the coefficient m_0^* in the expansion of Marangoni number is taken as $m_0^* = m_0 + \delta m_{01}$. This scaling works everywhere, except the vicinity of codimension-one region in parameter space, where the quadratic term changes its sign. The appropriate "slow" timescale is $\tau_1 = \delta\tau$, $\partial_\tau = \delta\partial_{\tau_1}$. We search the hexagonal solution at the first order of variable

TABLE I. Planform selection regions of Fig. 1.

Regions				
A1, A8	$\kappa_1 < 0$	$\kappa_1 + \kappa_2 < 0$	$\kappa_1 - \kappa_2 > 0$	stable supercritical rolls
A2	$\kappa_1 < 0$	$\kappa_1 + \kappa_2 < 0$	$\kappa_1 - \kappa_2 < 0$	stable supercritical squares
A3	$\kappa_1 < 0$	$\kappa_1 + \kappa_2 > 0$	$\kappa_1 - \kappa_2 < 0$	subcritical squares
A4, A7	$\kappa_1 > 0$	$\kappa_1 + \kappa_2 < 0$	$\kappa_1 - \kappa_2 > 0$	subcritical rolls
A5	$\kappa_1 > 0$	$\kappa_1 + \kappa_2 > 0$	$\kappa_1 - \kappa_2 > 0$	subcritical rolls and squares
A6	$\kappa_1 > 0$	$\kappa_1 + \kappa_2 > 0$	$\kappa_1 - \kappa_2 < 0$	subcritical rolls and squares
B1, B9	$\kappa_1 < 0$	$\kappa_1 + \kappa_2 < 0$	$\kappa_1 - \kappa_2 > 0$	stable supercritical rolls
B2, B10	$\kappa_1 < 0$	$\kappa_1 + \kappa_2 < 0$	$\kappa_1 - \kappa_2 < 0$	stable supercritical squares
B3, B11	$\kappa_1 < 0$	$\kappa_1 + \kappa_2 > 0$	$\kappa_1 - \kappa_2 < 0$	subcritical squares
B4, B8	$\kappa_1 > 0$	$\kappa_1 + \kappa_2 > 0$	$\kappa_1 - \kappa_2 < 0$	subcritical rolls and squares
B5, B7	$\kappa_1 > 0$	$\kappa_1 + \kappa_2 > 0$	$\kappa_1 - \kappa_2 > 0$	subcritical rolls and squares
B6	$\kappa_1 > 0$	$\kappa_1 + \kappa_2 < 0$	$\kappa_1 - \kappa_2 > 0$	subcritical rolls
C1	$\kappa_1 < 0$	$\kappa_1 + \kappa_2 < 0$	$\kappa_1 - \kappa_2 > 0$	stable supercritical rolls
C2, C7	$\kappa_1 < 0$	$\kappa_1 + \kappa_2 < 0$	$\kappa_1 - \kappa_2 < 0$	stable supercritical squares
C3, C8	$\kappa_1 < 0$	$\kappa_1 + \kappa_2 > 0$	$\kappa_1 - \kappa_2 < 0$	subcritical squares
C4	$\kappa_1 > 0$	$\kappa_1 + \kappa_2 > 0$	$\kappa_1 - \kappa_2 < 0$	subcritical rolls and squares
C5	$\kappa_1 > 0$	$\kappa_1 + \kappa_2 > 0$	$\kappa_1 - \kappa_2 > 0$	subcritical rolls and squares
C6	$\kappa_1 > 0$	$\kappa_1 + \kappa_2 < 0$	$\kappa_1 - \kappa_2 > 0$	subcritical rolls
D1	$\kappa_1 < 0$	$\kappa_1 + \kappa_2 < 0$	$\kappa_1 - \kappa_2 > 0$	stable supercritical rolls
D2	$\kappa_1 < 0$	$\kappa_1 + \kappa_2 < 0$	$\kappa_1 - \kappa_2 < 0$	stable supercritical squares
D3	$\kappa_1 < 0$	$\kappa_1 + \kappa_2 > 0$	$\kappa_1 - \kappa_2 < 0$	subcritical squares
D4, D7	$\kappa_1 > 0$	$\kappa_1 + \kappa_2 < 0$	$\kappa_1 - \kappa_2 > 0$	subcritical rolls
D5	$\kappa_1 > 0$	$\kappa_1 + \kappa_2 > 0$	$\kappa_1 - \kappa_2 > 0$	subcritical rolls and squares
D6	$\kappa_1 > 0$	$\kappa_1 + \kappa_2 > 0$	$\kappa_1 - \kappa_2 < 0$	subcritical rolls and squares

expansions as

$$h_1 = A_1(\tau_1, \tau_2)e^{iKX} + A_2(\tau_1, \tau_2)e^{(iK/2)(-X+\sqrt{3}Y)} + A_3(\tau_1, \tau_2)e^{(-iK/2)(X+\sqrt{3}Y)} + \text{c.c.}$$
$$f_1 = \alpha[A_1(\tau_1, \tau_2)e^{iKX} + A_2(\tau_1, \tau_2)e^{(iK/2)(-X+\sqrt{3}Y)} + A_3(\tau_1, \tau_2)e^{(-iK/2)(X+\sqrt{3}Y)}] + \text{c.c.} \quad (44)$$

Here "c.c." means complex conjugate terms, and $\alpha = 1 - 2(G + SK^2)/(3m_0)$.

Substituting solution (44) into the right-hand side of the equations at the second order in δ we obtain expressions containing three kinds of terms—two nonresonant with $\exp(2i\mathbf{K}_j \cdot \mathbf{R})$ and $\exp(i(\mathbf{K}_j - \mathbf{K}_m) \cdot \mathbf{R})$ and one term is a resonant with $\exp(i\mathbf{K}_n \cdot \mathbf{R})$. The solvability condition for the resonant term provides the following system of the amplitude equations:

$$\partial_{\tau_1} A_1 = \kappa_0 A_1 + n_1 A_2^* A_3^*, \quad (45)$$

$$\partial_{\tau_1} A_1 = \kappa_0 A_2 + n_1 A_3^* A_1^*, \quad (46)$$

$$\partial_{\tau_1} A_3 = \kappa_0 A_3 + n_1 A_1^* A_2^*. \quad (47)$$

Here the coefficient $\kappa_0 = (d\lambda/dM_m)m_{01}$. These equations describe the transcritical bifurcation of the hexagonal pattern which is unstable in both subcritical and supercritical region.

The coefficient n_1 can have different sign and that defines the type of hexagons in the subcritical region. Two types of hexagonal patterns are possible: $up - hexagons$ (H^+) with the relatively hot rising liquid in the center and sinking liquid near the hexagon boundary and $down - hexagons$ (H^-) with inverse circulation of a liquid. The boundary between the domains of definite kinds of hexagons

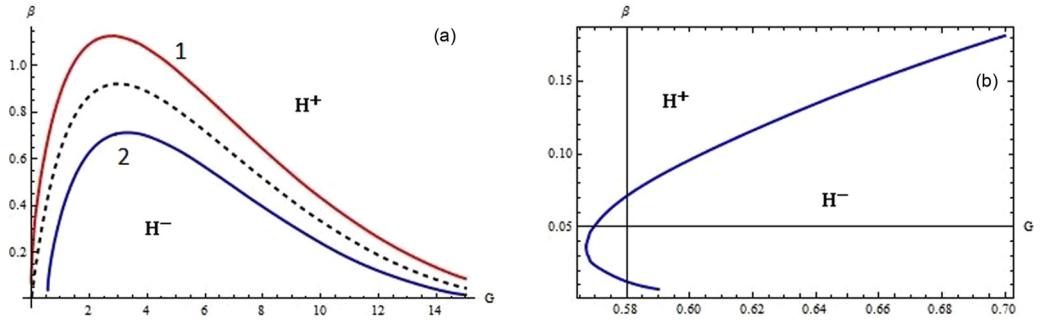

FIG. 2. Pattern selection on hexagonal lattice. H^- is a region of the subcritical bifurcation of down-hexagons, H^+ is a region of the subcritical bifurcation of up-hexagons. The dashed line is for $m_1 = 0$, line 1 (red line) is for $m_1 = 0.2$, and line 2 (blue line) is for $m_1 = -0.2$. Panel (b) is the map in the vicinity of the smallest values of β and G (case $m_1 = -0.2$).

in the subcritical region can be found, as $n_1 = 0$. At the critical monotonic Marangoni number and critical wavelength we have the following boundary:

$$3456\left(G + SK_{m,c}^2\right)\left[2K_{m,c}^2\left(G + SK_{m,c}^2 - 18\right) + 3\left(G + SK_{m,c}^2 + 12\right)\beta\right] - \frac{K_{m,c}^4 m_1\left(G + SK_{m,c}^2 + 72\right)^3}{K_{m,c}^2 + \beta} = 0. \tag{48}$$

Figure 2 shows pattern selection on the hexagonal lattice. The dashed line presents the boundary (48) for $m_1 = 0$. The red line presents the case when $m_1 = 0.2$. The blue line is for $m_1 = -0.2$. It is shown, that when coefficient m_1 increases the region of down-hexagons grows, and when this coefficient decreases, then the region of down-hexagons shrinks.

VI. OSCILLATORY MODE

A. Interaction of traveling waves

For the oscillatory mode we repeat the procedure described in the previous section. Figure 3 reconstructed from paper [13] presents the domain of long-wave oscillatory instability mode. The

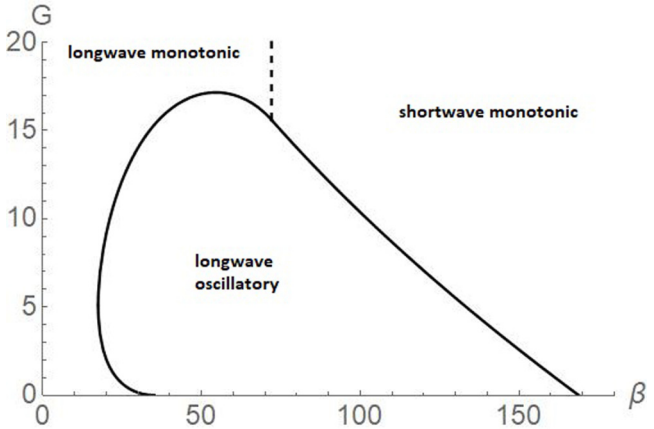

FIG. 3. The domain of oscillatory instability.

marginal stability curve of the oscillatory mode is determined by formula (23), the critical wave number is determined by formula (25). The bifurcation analysis can be done at any K, but the case of critical wave number is especially important. We remind that the oscillatory mode exists only if $M_o^{(b)}(K) < M_m^{(b)}(K)$. For the description of the Hopf bifurcation, we introduce $m_0^* = m_0 + \delta^2 m_{02}$ and $\tau_2 = \delta^2 \tau$.

To consider the nonlinear interaction of waves we take a pair of traveling waves with the wave vectors $\mathbf{K_1} = (K_1, 0)$ and $\mathbf{K_2} = (K\cos\theta, K\sin\theta)$. They propagate with a phase velocity $\pm\omega_0/K$, i.e.,

$$h_1 = H_1^{(1)}(\tau_2)e^{iKX+i\omega_0\tau_0} + H_1^{(2)}e^{iKX\cos\theta+iKY\sin\theta+i\omega_0\tau_0} + \text{c.c.}, \tag{49}$$

$$f_1 = \alpha\left(H_1^{(1)}(\tau_2)e^{iKX+i\omega_0\tau_0} + H_1^{(2)}e^{iKX\cos\theta+iKY\sin\theta+i\omega_0\tau_0}\right) + \text{c.c.}. \tag{50}$$

Here $\alpha = 1 - 2(G+SK^2)/(3m_0) - 2i\omega_0/(m_0K^2)$ and ω_0 is determined by (32). Note that this general case of two-wave interaction was not considered in Ref. [13].

At the second order in δ the solution can be taken as

$$\begin{aligned} h_2 = {} & H_2^{(1)}(\tau_2)e^{2iKX+2i\omega_0\tau_0} + H_2^{(2)}(\tau_2)e^{2iKX\cos\theta+2iKY\sin\theta+2i\omega_0\tau_0} \\ & + D_2^{(1)}(\tau_2)e^{iKX+iKX\cos\theta+iKY\sin\theta+2i\omega_0\tau_0} + D_2^{(2)}(\tau_2)e^{iKX-iKX\cos\theta-iKY\sin\theta} + \text{c.c.}, \end{aligned} \tag{51}$$

$$\begin{aligned} f_2 = {} & F_0 + F_2^{(1)}(\tau_2)e^{2iKX+2i\omega_0\tau_0} + F_2^{(2)}(\tau_2)e^{2iKX\cos\theta+2iKY\sin\theta+2i\omega_0\tau_0} \\ & + C_2^{(1)}(\tau_2)e^{iKX+iKX\cos\theta+iKY\sin\theta+2i\omega_0\tau_0} + C_2^{(2)}(\tau_2)e^{iKX-iKX\cos\theta-iKY\sin\theta} + \text{c.c.} \end{aligned} \tag{52}$$

The solvability condition applied at the third order determines the set of equations for the evolution of wave amplitudes in the form of the Landau equations [here $H^{(1)} = H_1^{(1)}$, $H^{(2)} = H_1^{(2)}$]:

$$\frac{dH^{(1)}}{d\tau_2} = \kappa_0 H^{(1)} + \kappa_1|H^{(1)}|^2H^{(1)} + \kappa_2(\theta)|H^{(2)}|^2H^{(1)}, \tag{53}$$

$$\frac{dH^{(2)}}{d\tau_2} = \kappa_0 H^{(2)} + \kappa_1|H^{(2)}|^2H^{(2)} + \kappa_2(\theta)|H^{(1)}|^2H^{(2)}. \tag{54}$$

In the latter case,

$$\kappa_0 = \left[\frac{K^2}{6} - \frac{iK^4(G+SK^2+72)}{288\omega_0}\right]m_{02}. \tag{55}$$

The coefficients κ_1 and $\kappa_2(\theta)$ are cumbersome to be given here.

B. Single traveling waves

We consider first the solution that consists of one single traveling wave [$H^{(2)} = 0$] with complex amplitude $H^{(1)}$, which we take in the polar form

$$H^{(1)} = R_1(\tau_2)e^{i\phi_1(\tau_2)}.$$

Here $R_1(\tau_2)$ and $\phi_1(\tau_2)$ are real functions. Substituting this polar form of $H^{(1)}$ into (53) we obtain for the real and imaginary parts, respectively,

$$\frac{dR_1}{d\tau_2} = \kappa_{0,r}R_1 + \kappa_{1,r}R_1^3, \quad \frac{d\phi_1}{d\tau_2} = \kappa_{0,i} + \kappa_{1,i}R_1^2. \tag{56}$$

Here $\kappa_{0,r}$ and $\kappa_{1,r}$ are real parts and $\kappa_{0,i}$ and $\kappa_{1.i}$ are imaginary parts of the coefficients κ_0 and κ_1, respectively. Note that $\kappa_{0,r} > 0$ in the supercritical region ($m_{02} > 0$) and $\kappa_{0,r} < 0$ in the subcritical region ($m_{02} < 0$). The first equation has one nontrivial fixed point

$$\left[R_1^{(0)}\right]^2 = -\frac{\kappa_{0,r}}{\kappa_{1,r}},$$

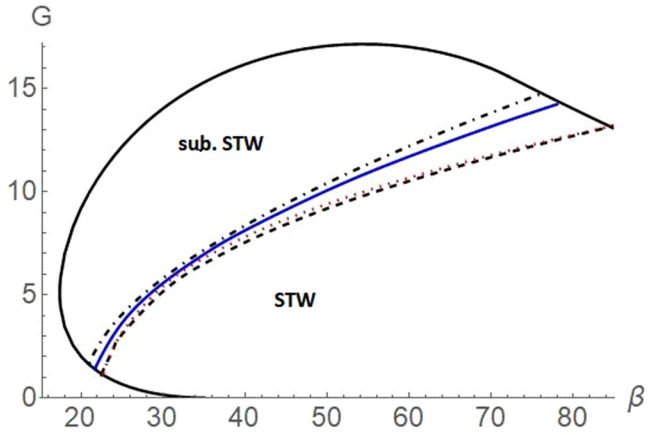

FIG. 4. Selection of oscillatory patterns on the square lattice. Solid line is for linear dependence of surface tension function. Dashed line is for $m_1 = 0.6m_0$, $m_2 = 0$; dot-dashed line is for $m_1 = -0.5m_0$, $m_2 = 0$; and dotted line is for $m_1 = 0.8m_0$, $m_2 = -0.3m_0$. Above these lines STW bifurcates subcritically.

corresponding to a single traveling wave (STW). The stability of this fixed point is determined by the sign of $\kappa_{0,r}$, see Ref. [20]. When $\kappa_{0,r} > 0$ and $\kappa_{1,r} < 0$ the STW is supercritical and stable (direct Hopf bifurcation). In the region where $\kappa_{0,r} < 0$ the solution exists if $\kappa_{1,r} > 0$; then the bifurcation of STW is subcritical, and the solution is unstable (inverse Hopf bifurcation). In the latter case, the weakly nonlinear analysis is not sufficient for finding nontrivial stable solutions of system (20) and (21).

Figure 4 shows the boundary between domains of the supercritical and subcritical bifurcation for STW. For illustration how the nonlinearity of surface tension function changes the subcritical and supercritical domains we use the following sets of parameters. (i) Linear dependence of surface tension function ($m_1 = m_2 = 0$, solid line on Fig. 4), (ii) $m_1 = 0.6m_0$, $m_2 = 0$ [here $m_0 = m_{osc}(K_c^o)$], dashed line on Fig. 4, (iii) $m_1 = -0.5m_0$, $m_2 = 0$, dot-dashed line on Fig. 4, and (iv) $m_1 = 0.8m_0$, $m_2 = -0.3m_0$, dotted line on Fig. 4.

C. Two-wave interaction under arbitrary angle

Here we consider the general case, when two waves propagate under arbitrary angle θ one to another. Using again the polar notation for the amplitudes in the system (53) and (54), $H^{(1)} = R_1(\tau_2)e^{i\phi_1(\tau_2)}$ and $H^{(2)} = R_2(\tau_2)e^{i\phi_2(\tau_2)}$, we obtain the following set of equations for real variables:

$$\frac{dR_1}{d\tau_2} = \kappa_{0,r}R_1 + \kappa_{1,r}R_1^3 + \kappa_{2,r}(\theta)R_2^2R_1, \tag{57}$$

$$\frac{dR_2}{d\tau_2} = \kappa_{0,r}R_2 + \kappa_{1,r}R_2^3 + \kappa_{2,r}(\theta)R_1^2R_2, \tag{58}$$

$$\frac{d\phi_1}{d\tau_2} = \kappa_{0,i} + \kappa_{1,i}R_1^2 + \kappa_{2,i}(\theta)R_2^2, \tag{59}$$

$$\frac{d\phi_2}{d\tau_2} = \kappa_{0,i} + \kappa_{1,i}R_2^2 + \kappa_{2,i}(\theta)R_1^2. \tag{60}$$

Equations (57) and (58) have the following fixed points:

(i) $R_1^{(0)} = R_2^{(0)} = 0$ (quiescent state),

(ii) $[R_1^{(0)}]^2 = -\kappa_{0,r}/\kappa_{1,r}$ and $R_2 = 0$ or vice versa (STW),

(iii) $[R_1^{(0)}]^2 = [R_2^{(0)}]^2 = -\kappa_{0,r}/[\kappa_{1,r} + \kappa_{2,r}(\theta)]$ (TR).

In the case $\theta = \pi$ the waves move in opposite directions and form a standing wave.

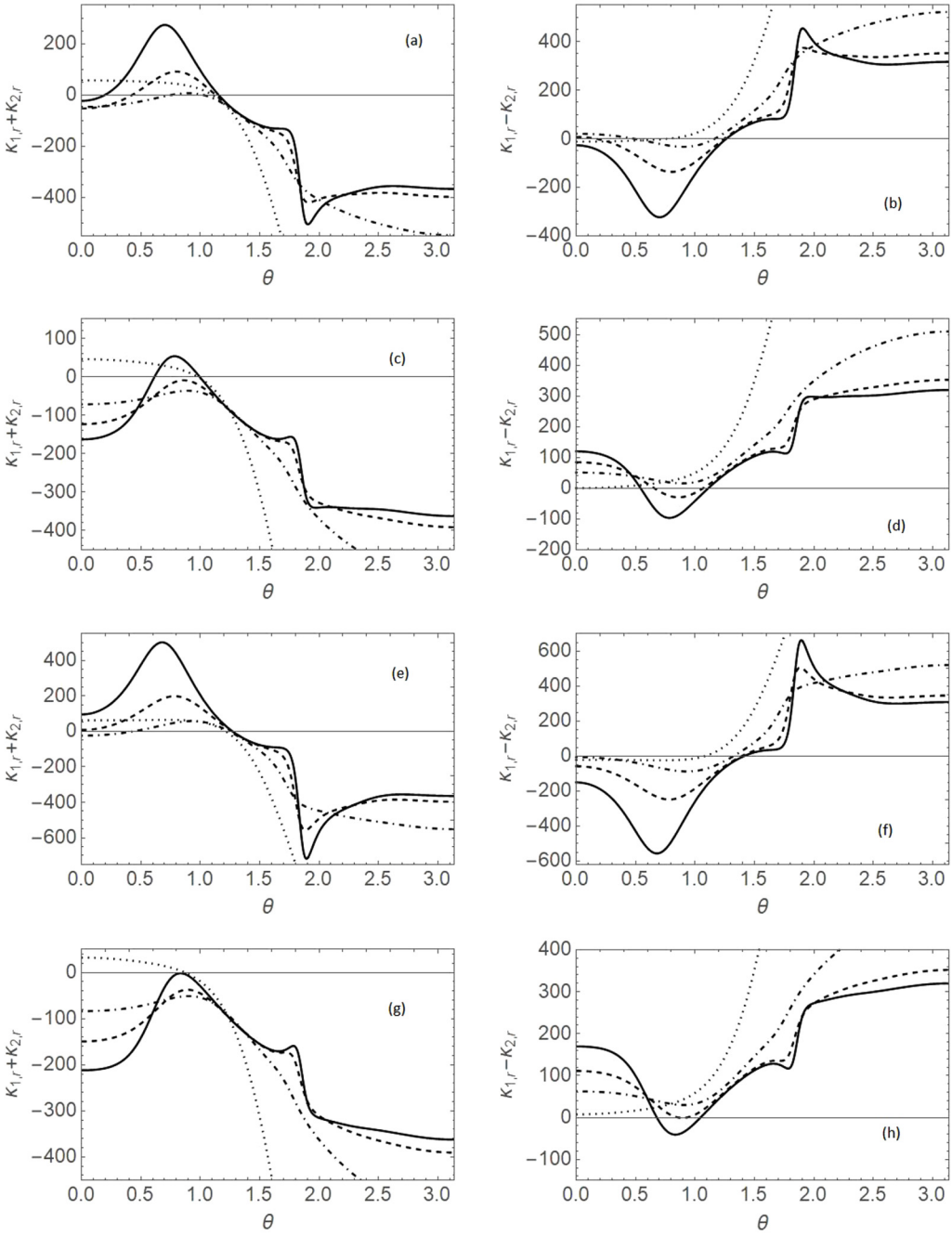

FIG. 5. $\kappa_{1,r} \pm \kappa_{2,r}(\theta)$ vs. angle θ for $\beta = 30$ and $G = 0.5$ (solid line), $G = 1$ (dashed line), $G = 3$ (dot-dashed line), and $G = 10$ (dotted line). [(a) and (b)] For $m_1 = m_2 = 0$, [(c) and (d)] for $m_1 = 0.6m_0$ and $m_2 = 0$, [(e) and (f)] for $m_1 = -0.5m_0$ and $m_2 = 0$, and [(g) and (h)] for $m_1 = 0.8m_0$ and $m_2 = -0.3m_0$.

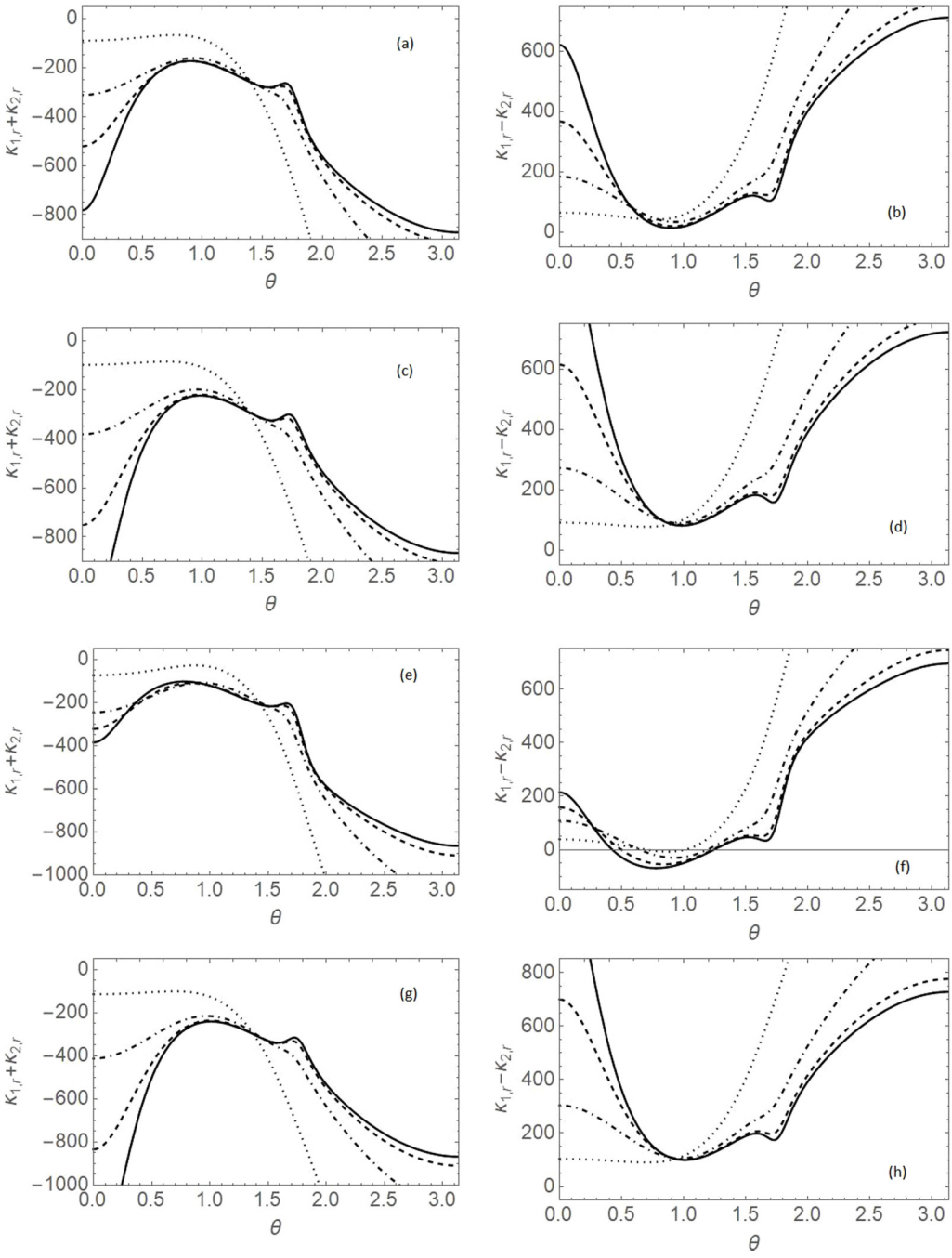

FIG. 6. $\kappa_{1,r} \pm \kappa_{2,r}(\theta)$ vs. angle θ for $\beta = 60$ and $G = 0.5$ (solid line), $G = 1$ (dashed line), $G = 3$ (dot-dashed line), and $G = 10$ (dotted line). [(a) and (b)] For $m_1 = m_2 = 0$, [(c) and (d)] for $m_1 = 0.6m_0$ and $m_2 = 0$, [(e) and (f)] for $m_1 = -0.5m_0$ and $m_2 = 0$, and [(g) and (h)] for $m_1 = 0.8m_0$ and $m_2 = -0.3m_0$.

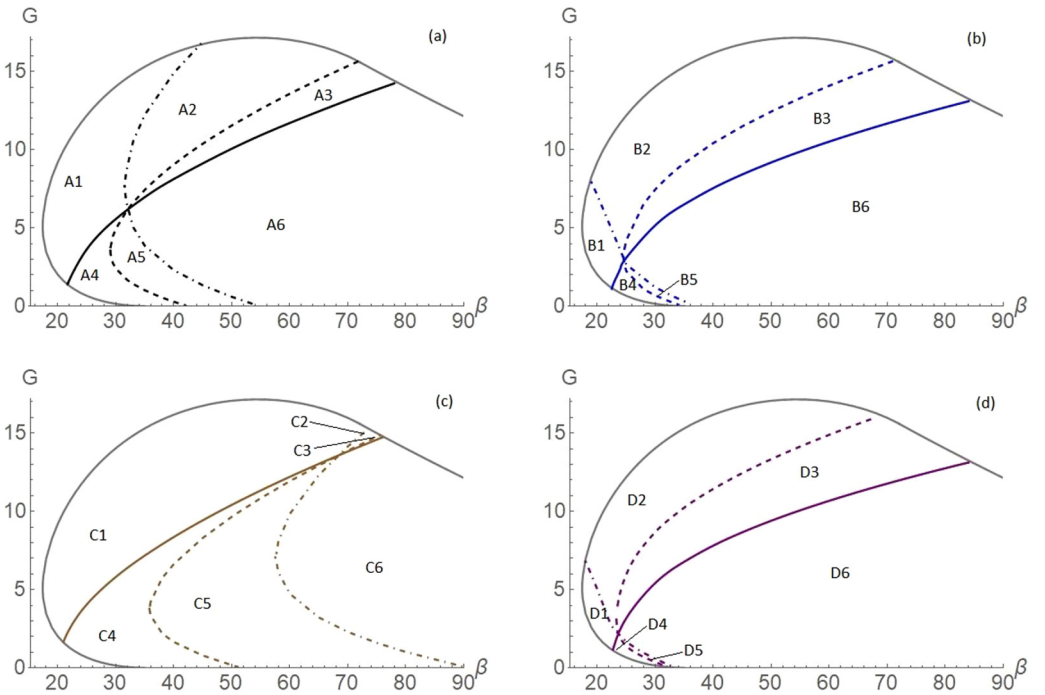

FIG. 7. Pattern selection domains for oscillatory mode when $\theta = 0.702$ for (a) $m_1 = m_2 = 0$ (linear case). (b) $m_1 = 0.6m_0$ and $m_2 = 0$, (c) $m_1 = -0.5m_0$ and $m_2 = 0$, and (d) $m_1 = 0.8m_0$ and $m_2 = -0.3m_0$. Here solid line is for $\kappa_{1,r} = 0$, dashed line is for $\kappa_{1,r} + \kappa_{2,r} = 0$, and dot-dashed line is for $\kappa_{1,r} - \kappa_{2,r} = 0$.

If $\kappa_{1,r} > 0$ or $\kappa_{1,r} + \kappa_{2,r} > 0$, then the system has no stable nontrivial stationary solutions. The supercritical STW exists for $\kappa_{1,r} < 0$, when $\kappa_{1,r} + \kappa_{2,r}(\theta) < 0$ we have supercritical TR. In the case where both STW and TR bifurcate in a supercritical way, only one type of waves is stable: (i) If $\kappa_{1r} > \kappa_{2r}$, then the stable solutions are STW; (ii) if $\kappa_{1r} < \kappa_{2r}$, then the stable solution is TR.

Here the coefficient κ_2 depends on the propagation angle θ with respect to the another wave. Therefore, the angle θ is additional parameter to the pair (β, G). The way of bifurcation and selection of a two-wave pattern are determined by $\kappa_{1,r} \pm \kappa_{2,r}(\theta)$. First, we draw the graphs of $\kappa_{1,r} \pm \kappa_{2,r}(\theta)$ for different angles at fixing values of the pair (β, G). Figure 5 presents the graphs at fixed $\beta = 30$ and different G: $G = 0.5$ (solid line), $G = 1$ (dashed line), $G = 3$ (dot-dashed line), and $G = 10$ (dotted line). Figure 5 shows that the maximum of $\kappa_{1,r} + \kappa_{2,r}(\theta)$ depends on parameters. For instance, for linear dependence of surface tension function on temperature (case $m_1 = m_2 = 0$) the maximum of $\kappa_{1,r} + \kappa_{2,r}(\theta) = 273.1$ at $\theta_{\max} = 0.702$ $(G = 0.5)$. When $m_1 = 0.6m_0$, $m_2 = 0$ the maximum of $\kappa_{1,r} + \kappa_{2,r}(\theta) = 53.44$ at $\theta_{\max} = 0.784$ $(G = 0.5)$, when $m_1 = -0.5m_0$, $m_2 = 0$ the maximum of $\kappa_{1,r} + \kappa_{2,r}(\theta) = 502.2$ at $\theta_{\max} = 0.679$ $(G = 0.5)$, and when $m_1 = 0.8m_0$ and $m_2 = -0.3m_0$ the maximum of $\kappa_{1,r} + \kappa_{2,r}(\theta) = 32.31$ at $\theta_{\max} = 0$ $(G = 10)$.

Similar results obtained for $\beta = 60$ are presented in Fig. 6.

To describe the planform selection for two-wave interaction we fix the angle of interaction at $\theta = 0.702$ and then for fixed values m_1 and m_2 we plot the diagrams of stability domains for the oscillatory mode, see Fig. 7. As in the case of the monotonic mode here we divide the whole domain of oscillatory instability into six regions. On each panel, the regions are presented for a fixed couple of parameters m_1 and m_2. Figure 7(a) shows regions A1-A6 for $m_1 = 0$ and $m_2 = 0$ (this is case of linear surface tension function); Fig. 7(b) shows regions B1–B6 for $m_1 = -0.6m_0$, $m_2 = 0$; Fig. 7(c) with regions C1–C6 represents planform selection for $m_1 = -0.5m_0$ and $m_2 = 0$, and Fig. 7(d) shows regions D1–D6 for $m_1 = 0.8m_0$ and $m_2 = -0.3m_0$. On each plot the solid line

TABLE II. Regular wave patterns in Fig. 7.

Regions				
A1, B1, C1, and D1	$\kappa_{1,r} > 0$	$\kappa_{1,r} + \kappa_{2,r} > 0$	$\kappa_{1,r} - \kappa_{2,r} < 0$	subcritical STW and TR
A2, B2, C2, and D2	$\kappa_{1,r} > 0$	$\kappa_{1,r} + \kappa_{2,r} > 0$	$\kappa_{1,r} - \kappa_{2,r} > 0$	subcritical TR and STW
A3, B3, C3, and D3	$\kappa_{1,r} > 0$	$\kappa_{1,r} + \kappa_{2,r} < 0$	$\kappa_{1,r} - \kappa_{2,r} > 0$	subcritical STW
A4, B4, C4, and D4	$\kappa_{1,r} < 0$	$\kappa_{1,r} + \kappa_{2,r} > 0$	$\kappa_{1,r} - \kappa_{2,r} < 0$	subcritical TR
A5, B5, C5, and D5	$\kappa_{1,r} < 0$	$\kappa_{1,r} + \kappa_{2,r} < 0$	$\kappa_{1,r} - \kappa_{2,r} < 0$	stable supercritical TR
A6, B6, C6, and D6	$\kappa_{1,r} < 0$	$\kappa_{1,r} + \kappa_{2,r} < 0$	$\kappa_{1,r} - \kappa_{2,r} > 0$	stable supercritical STW

depicts the boundary $\kappa_{1,r} = 0$, the dashed line is the line where $\kappa_{1,r} + \kappa_{2,r} = 0$, and the dash-dotted line corresponds to the condition $\kappa_{1,r} - \kappa_{2,r} = 0$. The results are summarized in Table II.

We did not find stable standing waves at $\theta = \pi$ on the square lattice for the oscillatory mode.

VII. SUMMARY

Traditionally in the problems describing the Marangoni convection the surface tension is considered as a linear function of temperature. However, a lot of experimental works (see Refs. [2–11]) show that in some situations the surface tension is a nonlinear function on temperature that we describe by the set of Taylor's expansion coefficients. This approach is applied to the problem of long-scale thermocapillary convection in the case of weak heat flux from the free liquid surface (the problem was first considered by Shklyaev *et al.* in Ref. [13]), where the instability of the motionless state can be caused by both monotonic and oscillatory instability modes.

Rewriting the set of evolution equations for surface deflection and temperature perturbations for the arbitrary nonlinear dependence of the surface tension on temperature we applied the weakly nonlinear analysis and considered the pattern selection in the case of monotonic instability mode, as well as the wave patterns in the case of oscillatory mode. The influence of the temperature dependence nonlinearity of the surface tension on the formation and evalution of the patterns is the novelty of this investigation. We have shown that the type of bifurcation and pattern selection cannot be determined correctly without taking into account two Taylor's expansion coefficients characterizing that nonlinearity. The coefficients in the surface tension function expansion were taken from experimental data published in the papers. Also, we have investigated the influence of those coefficients on the pattern stability that could be used in future experiments.

The analysis of the problem shows that supercritical excitation is possible for both steady and oscillatory convection. Depending on parameters in the steady case the rolls or squares can be selected. Different dependence of the surface tension function on temperature gives different pattern selection and influence on the stability of rolls against squares. Hexagons of two types, up-hexagons and down-hexagons, can be selected in the steady case as well. Among the oscillatory patterns single traveling waves as well as traveling rectangles were considered. The influence of nonlinearity of the surface tension function on these regular waves was demonstrated.

To our knowledge, there are no much experiments on the deformational mode of the Marangoni instability beyond the already classical works of Schatz *et al.* [21,22], who showed that this instability leads to the rupture of the film. We believe that the results of this work could stimulate future experiments in real systems with strong dependence of the surface tension on the temperature and estimate the values of parameters (thickness, temperature gradient, etc.) such that the effects described in the present paper can be observed.

An approach similar to that described in this paper can be applied to the solutocapillary convection in the case when the surface tension function depends nonlinearly on the concentration of surfactant. Results of this paper can be used as a good reference point for future numerical simulation of the total system of equations.

ACKNOWLEDGMENT

A.A.N. acknowledges the support by the Israel Science Foundation (Grant No. 843/18).

APPENDIX: COEFFICIENTS A_2, B_2, D_2, F_{02}, C_1, C_2, AND C_3

$$(A_2, B_2) = -\frac{\left(A_1^2, B_1^2\right)(G+SK^2)[8K^2(G+SK^2-45)+3(48+5G+5SK^2)\beta]}{12[G(72+G)\beta+5GSK^2\beta+4SK^4(S\beta-72)]} + \frac{\left(A_1^2, B_1^2\right)K^4 m_1(72+G+SK^2)^3(4K^2+\beta)}{41472(K^2+\beta)^2[G(72+G)\beta+5GSK^2\beta+4K^4S(S\beta-72)]}, \tag{A1}$$

$$D_2 = -\frac{A_1B_1(G+SK^2)[4K^2(G+SK^2-36)+(72+7G+7SK^2)\beta]}{G(72+G)\beta+3GSK^2\beta+2SK^4(S\beta-72)} + \frac{A_1B_1K^4m_1(72+G+SK^2)^3(2K^2+\beta)}{3456(K^2+\beta)^2[G(72+G)\beta+3GSK^2\beta+2SK^4(S\beta-72)]}, \tag{A2}$$

$$F_{02} = -\frac{K^2}{4\beta}\left(A_1^2+B_1^2\right), \tag{A3}$$

$$(C_1, C_2) = \frac{\left(A_1^2, B_1^2\right)\mathcal{D}_1}{216(k^2+\beta)[G(72+G)\beta+5GSK^2\beta+4SK^2(S\beta-72)]} - \frac{\left(A_1^2, B_1^2\right)K^4m_1(72+G+SK^2)^3(GK^2+4SK^4-18\beta)}{746496(K^2+\beta)^2[G(72+G)\beta+5GSK^2\beta+4SK^4(S\beta-72)]}, \tag{A4}$$

$$\mathcal{D}_1 = 2K^4\{-1944SK^2+(G+SK^2)[(G-45)G+(144+5G)SK^2+4S^2K^4]\} + 3K^2\{G[864+(G-72)G]+6[792+G(21+G)]SK^2+9(22+G)S^2K^4+4K^6S^3\}\beta - 54(G+SK^2)(48+5G+5SK^2)\beta^2, \tag{A5}$$

$$C_3 = \frac{A_1B_1\mathcal{D}_2}{36(K^2+\beta)[G(72+G)\beta+3GK^2S\beta+2K^4S(S\beta-72)]} - \frac{A_1B_1K^4m_1(72+G+SK^2)^3(GK^2+2SK^4-36\beta)}{124416(K^2+\beta)^2[G(72+G)\beta+3GSK^2\beta+2K^4S(S\beta-72)]}, \tag{A6}$$

$$\mathcal{D}_2 = 2K^4(G+K^2)[(G-36)G+3(12+G)SK^2+2S^2K^4]+3K^2\{(G-36)(G-24)G + 4[648+(G-6)G]SK^2+(5G+36)S^2K^4+2S^3K^6\}\beta-36(G+SK^2)(72+7G+7SK^2)\beta^2. \tag{A7}$$

Here (A1) and (A4) are written for the pairs of coefficients.

[1] S. H. Davis, Thermocapillary instabilities, Annu. Rev. Fluid Mech. **19**, 403 (1987).
[2] G. Petre, M. A. Azouni, and K. Tshinyama, Marangoni convection at alcohol aqueous solutions-air interfaces, Appl. Sci. Res. **50**, 97 (1993).
[3] J. C. Legros, M. C. Limbourg-Fontaine, and G. Petre, Influence of a surface tension minimum as a function of temperature on the Marangoni convection, Acta Astronaut. **11**, 143 (1984).
[4] M. C. Limbourg-Fontaine, G. Petre, J. C. Legros, and E. Van Ransbeeck, Thermocapillary movements around a surface tension minimum under microgravity conditions (Part 1. Technical description of STEM experiments. D_1mission of Spacelab), Acta Astronaut. **13**, 197 (1986).
[5] J. C. Legros, Problems related to non-linear variations of surface tension, Acta Astronaut. **13**, 697 (1986).

[6] N. Eustathopoulos, J. C. Joud, P. Desre, and J. M. Hicter, The wetting of carbon by aluminium and aluminium alloys, J. Mater. Sci. **9**, 1233 (1974).
[7] E. Guyon and J. Pantaloni, Effet de tension superficielle sur la convection de Rayleigh-Benárd, C. R. Acad. Sci. Paris B **290**, 301 (1980).
[8] A. Cloot and G. Lebon, Marangoni convection induced by a nonlinear temperature-dependent surface tension, J. Phys. Paris **47**, 23 (1986).
[9] Yu. P. Gupalo and Yu. S. Ryazantsev, Thermocapillary motion of a liquid with a free surface with nonlinear dependence of the surface tension on the temperature, Fluid Dyn. **23**, 752 (1989).
[10] A. Oron and P. Rosenau, On a nonlinear thermocapillary effect in thin liquid layers, J. Fluid Mech. **273**, 362 (1994).
[11] S. G. Slavtchev and S. P. Miladinova, Thermocapillary flow in a liquid layer at minimum in surface tension, Acta Mech. **127**, 209 (1998).
[12] A. Podolny, A. Oron, and A. Nepomnyashchy, Long-wave Marangoni instability in a binary-liquid layer with deformable interface in the presence of Soret effect: Linear theory, Phys. Fluids **17**, 104104 (2005).
[13] S. Shklyaev, A. A. Alabuzhev, and M. Khenner, Long-wave Marangoni convection in a thin film heated from below, Phys. Rev. E **85**, 016328 (2012).
[14] R. Sarma and P. K. Mondal, Marangoni instability in a thin film heated from below: Effect of nonmonotonic dependence of surface tension on temperature, Phys. Rev. E **97**, 043105 (2018).
[15] A. B. Mikishev and A. A. Nepomnyashchy, Amplitude equations for large-scale Marangoni convection in a liquid layer with insoluble surfactant on deformable free surface, Microgravity Sci. Technol. **23**, 59 (2010).
[16] A. B. Mikishev and A. A. Nepomnyashchy, Weakly nonlinear analysis of long-wave Marangoni convection in a liquid layer covered by insoluble surfactant, Phys. Rev. Fluids **4**, 094002 (2019).
[17] D. Villers and J. K. Platten, Thermal convection in superposed immeiscible liquid layers, Appl. Sci. Res. **45**, 145 (1988).
[18] D. R. Jenkins, Rolls versus squares in thermal convection of fluids with temperature-dependent viscosity, J. Fluid Mech. **178**, 491 (1987).
[19] F. H. Busse, The stability of finite amplitude cellular convection and its relation to an extremum principle, J. Fluid Mech. **30**, 625 (1967).
[20] A. Podolny, A. Oron, and A. A. Nepomnyashchy, Linear and nonlinear theory of long-wave Marangoni instabilitywith the Soret effect at finite Biot numbers, Phys. Fluids **18**, 054104 (2006).
[21] M. F. Schatz, S. J. VanHook, W. D. McCormick, J. B. Swift, and H. L. Swinney, Onset of Surface-Tension-Driven Bénard Convection, Phys. Rev. Lett. **75**, 1938 (1995).
[22] S. J. VanHook, M. F. Schatz, J. B. Swift, W. D. McCormick, and H. L. Swinney, Long-wavelength surface-tension-driven Bénard convection: Experiment and theory, J. Fluid Mech. **345**, 45 (1997).